Measurement of Spin-Wave Dispersion in NiO by Inelastic Neutron Scattering and Its Relation to Magnetic Properties

M. T. Hutchings
Brookhaven National Laboratory, Upton, New York* 11973
and AERE Harwell, Didcot, Berkshire, England†

and

E. J. Samuelsen‡
Brookhaven National Laboratory, Upton, New York* 11973
(Received 12 June 1972)

Inelastic neutron scattering techniques have been used to measure the spin-wave dispersion relations at 78 °K in the fcc antiferromagnet NiO. The energy dispersion has a steep initial slope (~ 250 meV Å) and a high maximum energy (~ 117 meV) and is further characterized by a relatively low zone boundary energy in certain directions. The exchange parameters defined by $\mathcal{H}^{1,2} = J_f \vec{S}^{(1)} \cdot \vec{S}^{(2)}$ were determined by fitting the theoretical expression for the spin-wave energies to the experimental data corrected for instrumental resolution effects. The predominant interaction is a large antiferromagnetic exchange $J_2 = 221$ °K (19.01 meV) between next-nearest neighbors, which are linked by a 180° superexchange path. The interaction between nearest neighbors, linked by a 90° Ni^{2+}—O^{2-}—Ni^{2+} configuration, is much smaller and ferromagnetic in sign, $J_1 = -15.9$ °K (−1.37 meV). A consequence of the relatively small value of J_1 is that the spin waves from the four domains present in the sample can only be resolved in a limited region of reciprocal space. These values of exchange interactions are in accord with simple ideas of covalency and overlap, and the results emphasize the behavior of NiO as a weakly covalent insulator. The density of magnon states, estimates of the transition temperature, and several thermomagnetic properties of NiO have been calculated from the measured exchange parameters using molecular field and random-phase-approximation Green's-function formulas.

I. INTRODUCTION

A detailed knowledge of the exchange interactions in fcc nickel oxide is of fundamental importance in the theory of antiferromagnetism in insulators, for three reasons. First, the nearest-neighbor (nn) and next-nearest-neighbor (nnn) Ni^{2+} ions in this compound are connected, respectively, by simple 90° and 180° Ni^{2+}—O^{2-}—Ni^{2+} paths involving one intermediate O^{2-} ion. The magnitude of the superexchange interactions between ions interacting in this manner has been the subject of considerable theoretical work which ranges from qualitative estimates based on orbital overlap and covalency to more detailed quantitative calculations.[1] Second, the types of magnetic order and the magnetic properties of the fcc antiferromagnet have received much theoretical attention.[2–5] Nickel oxide is a prototype fcc antiferromagnet and below the Néel temperature $T_N = 523$ °K[6] orders in a type-II fcc spin pattern.[7–10] A knowledge of the magnetic interactions present enables different theoretical models for this structure to be tested by a comparison of the calculated static magnetic properties with experiment. Third, NiO is of current interest in the context of the metal–nonmetal transition problem. Simple band theory predicts NiO to be a metal, and the question of why it is not has received a great deal of attention.[11] As we shall see, the nature and magnitude of the experimentally determined exchange interactions help to characterize this compound as a weakly covalent insulator.

Prior to the present work only rough experimental estimates for the exchange and anisotropy parameters in NiO were available.[12–14] In order to obtain more accurate values we have therefore investigated the spin-wave dispersion relations at 78 °K using inelastic neutron scattering techniques.[15] The high Néel temperature indicates that there are large interactions between the ions, and these give rise to a steep initial slope to the dispersion (~ 250 meV Å) and a high maximum energy (~ 117 meV) (1 meV = 11.60 °K = 8.068 cm^{-1}). The measurement of these presents difficulties requiring special techniques to overcome. A further complication arises from the presence of four principal domains in the sample. In practice the inelastic scattering from these could only be separated at a few points in the Brillouin zone.

Recently Raman scattering data on NiO have been published[16] and confirm the conclusions of this neutron work. Two other fcc antiferromagnets, MnO and CoO, have been studied by inelastic neutron scattering. Complete data on MnO have very recently been taken by two groups[17,18] and show several similar features to those found in NiO. The magnetic scattering observed in CoO takes the form

of a broad band of intensity over a range of energy throughout the zone.[19] This is possibly due to lack of sufficiently good instrumental resolution to resolve the scattering from the individual domains.

In Sec. II of this paper we describe the crystal and magnetic structure of NiO, and in Sec. III we give the spin Hamiltonian and the theoretical expressions for the spin-wave energies. The experiments are described and the results are presented in Sec. IV. In Sec. V we comment on the results and compare with experiment a number of thermomagnetic properties calculated from the measured interactions using molecular field and random-phase-approximation (RPA) Green's-function theory. The conclusions are summarized in Sec. VI.

II. CRYSTAL AND MAGNETIC STRUCTURE

The crystal and magnetic structures of NiO have been the subject of a large number of detailed investigations using a variety of techniques. From x-ray diffraction work Rooksby[20] and Slack[21] find that an anisotropic lattice contraction and a rhombohedral distortion from the fcc structure set in at the Néel temperature and increase as the temperature is lowered. The distortion consists of a contraction along the [111] direction, and results in a change of cell angle from 90° above T_N to 90° 4′ at 297 °K and 90°6′ at 78 °K. Because there are four distinct ⟨111⟩ directions this will lead to the formation of four twin domains in a sample. The authors give the lattice constant $a_0 = 4.177$ Å at 297 °K and 4.1715 Å at 78 °K. Recently Bartel and Morosin[14] have made further x-ray measurements and found a slightly smaller change in the cell angle $\alpha = \frac{1}{2}\pi + \Delta$. They determine $a_0 = 4.1758$ Å and $\Delta = 3.5'$ at 297 °K, and $a_0 = 4.1705$ Å and $\Delta = 4.5'$ as $T \to 0$ °K. They also conclude that the magnetic interactions[22] contribute only very slightly to the isotropic part of the lattice contraction below T_N, but can account fully for the variation of Δ.

As far as the present neutron work is concerned this distortion is too small to be observed, and we may treat the lattice as pseudocubic. It does, however, have a bearing on the nn exchange and a marked effect on the spin-wave spectrum, as we shall see.

The magnetic structure of NiO was first investigated with powder neutron diffraction by Shull, Strauser, and Wollan,[7] and further detailed neutron work has been carried out by Roth[8,9] and by Roth and Slack.[10] Other techniques, such as bulk magnetic property measurements[23] and optical birefringence[24,25] have also been used to study the domain patterns in NiO, and have helped to elucidate the magnetic spin pattern. The magnetic structure is now firmly established as type-II fcc, that is, ferromagnetic sheets of spins in (111) planes, antiferromagnetically stacked along the ⟨111⟩ directions, as shown in Fig. 1. The moments lie within the (111) planes, and there is now considerable evidence that they lie in the $\langle 11\bar{2}\rangle$ directions.[25–28] The crystal distortion is directly related to the magnetic structure in that the contraction takes place perpendicular to the ferromagnetic layers, and an untreated crystal will contain 24 distinct kinds of domains. These are the four principal T domains corresponding to the four possible ⟨111⟩ directions, and a further three S domains corresponding to the three possible $\langle 11\bar{2}\rangle$ directions within each {111} plane. There will also be domains corresponding to a reversal of spin direction in each of the above.

The four T domains in a multiple-domain sample give rise to different magnetic Bragg peaks, and the rules for observation of peaks from each are summarized in Table I. Throughout this paper we shall index peaks on the reciprocal lattice of a simple cubic lattice of side $2a_0$. Neither the elastic nor inelastic scattering from different S domains could be distinguished. The nuclear reciprocal-lattice points are common to all domain types in the pseudocubic approximation, $\Delta \sim 0°$, and all have a finite structure factor. Indexed on our pseudocubic cell, they are at $\vec{\tau}_n = (\pi/a_0)(h, k, l)$, where h, k, and l are all of the form $4m$, or all of the form $4m+2$, and m can differ for each of h, k, or l. The magnetic reciprocal lattice for each T domain consists of the nuclear points plus the appropriate additional points listed in Table I,

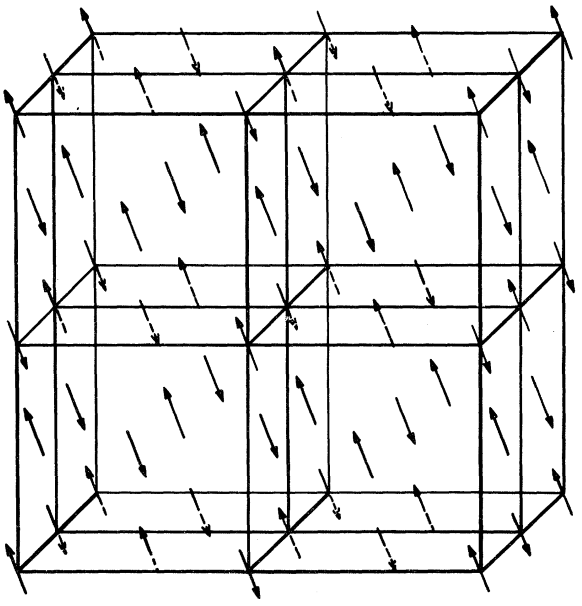

FIG. 1. Type-II fcc magnetic structure of domain A, NiO.

TABLE I. Magnetic intensity is observed at points $\vec{\tau}_m = (\pi/a_0)(h,k,l)$, where h,k,l are given below for each domain. m_1, m_2, and m_3 can be any integer but either the upper or lower sign must be taken for all three indices.

Domain A (111)	$h = 4m_1 \pm 1$	Domain B ($1\bar{1}\bar{1}$)	$h = 4m_1 \pm 1$
	$k = 4m_2 \pm 1$		$k = 4m_2 \pm 1$
	$l = 4m_3 \pm 1$		$l = 4m_3 \mp 1$
Domain C ($1\bar{1}1$)	$h = 4m_1 \pm 1$	Domain D ($\bar{1}11$)	$h = 4m_1 \mp 1$
	$k = 4m_2 \mp 1$		$k = 4m_2 \pm 1$
	$l = 4m_3 \pm 1$		$l = 4m_3 \pm 1$

which are those with finite magnetic structure factors. As an example, the reciprocal lattice of domain A is shown in Fig. 2, together with the first Brillouin zone. It is important to note that for a multi-T-domain sample the zones for each domain type may be centered at different reciprocal-lattice points when indexed as above. Consequently, the zone center of one domain type may coincide with the zone boundary of another. The zones in the $(1\bar{1}0)$ plane, shown in Fig. 3, illustrate this point.

III. THEORY

A. Spin Waves in NiO

We shall treat the Ni^{2+} ions in NiO in the weak-field approximation.[30] The octahedral cubic field splits the lowest $(3d)^8$ ^3F term into two upper orbital triplets and a lower-lying orbital singlet. This ground singlet state has threefold spin degeneracy, and the spin-orbit interaction will give rise to a small orbital contribution to the moment through admixture of the upper states ~ 13000 °K (~ 1100 meV) above in energy. Furthermore, it will cause a small splitting of the spin degeneracy should the symmetry become lower than cubic. In such a case of nearly-free-spin moments we would expect the exchange interactions between the ions to be very well described by the Heisenberg Hamiltonian.

The anisotropy in the fcc type-II antiferromagnet has been discussed by Kaplan,[31] by Keffer and O'Sullivan,[32] and by Yamada.[26] They show that the dipolar interactions will cause the spins to lie in the $\{111\}$ planes, and it seems likely that this is the major part of their "out-of-plane" anisotropy. A further contribution can arise from the rhombohedral distortion of the crystal field via the spin-orbit interaction. There is also a weaker "in-plane" anisotropy constraining the spins to the $\langle 11\bar{2} \rangle$ directions. The full effects of dipolar interactions on the spin-wave spectrum of an antiferromagnet can be quite complicated, giving rise to wave-vector-dependent contributions to the energies.[33] However, in NiO, the size of these effects is very small compared with that of the exchange interactions, and we shall represent all the anisotropy in terms of two constants D_1 and D_2. These describe the out-of-plane and in-plane anisotropies, respectively, and give rise to energy contributions which are wave-vector independent.

We therefore take our Hamiltonian for a given domain to be of the same form as that of Lines[4] in his treatment of MnO, but with $S = 1$,

$$\mathcal{H} = \sum_{j} \sum_{<i,\delta_j>} J_j \vec{S}_i \cdot \vec{S}_{i+\delta_j} + \sum_i D_1 (S_i^x)^2 + \sum_i D_2 (S_i^y)^2 \ . \tag{1}$$

Here z lies along the spin direction, and x is perpendicular to the ordering plane. $\langle i, \delta_j \rangle$ denotes the summation over all distinct pairs of jth-neighbor ions at $\vec{r}_i$ and $\vec{r}_i + \vec{\delta}_j$ coupled through an exchange interaction J_j. The index j is defined to increase with separation $|\vec{\delta}_j|$.

The number z_j of neighbors of type j with interaction J_j are listed in Table II. Due to the rhombohedral distortion, the 12 nearest neighbors which are equivalent above T_N become split into two sets of six below T_N. Following Lines[4] we denote them below T_N by J_1^+ and J_1^-, where the plus sign denotes coupling between antiparallel neighbors and the minus sign between parallel neighbors. We shall ignore such inequivalences between more distant neighbors.

Following conventional procedures[34] the spin-wave energies may be shown to be

$$\begin{aligned} E_1(\vec{q})^2 &= S^2(A_{\vec{q}} - B_{\vec{q}} + 2\eta D_1)(A_{\vec{q}} + B_{\vec{q}} + 2\eta D_2) \ , \\ E_2(\vec{q})^2 &= S^2(A_{\vec{q}} - B_{\vec{q}} + 2\eta D_2)(A_{\vec{q}} + B_{\vec{q}} + 2\eta D_1) \ , \end{aligned} \tag{2}$$

where

$$A_{\vec{q}} = \sum_j^{\parallel} \sum_{\delta_j} J_j e^{i\vec{q}\cdot\vec{\delta}_j} + \sum_j^{a\parallel} z_j J_j - \sum_j^{\parallel} z_j J_j$$

and

$$B_{\vec{q}} = \sum_j^{a\parallel} \sum_{\delta_j} J_j e^{i\vec{q}\cdot\vec{\delta}_j} \ .$$

The $\parallel$ and $a\parallel$ above the summation denote the sum over parallel or antiparallel spins. The anisotropy terms require some separate discussion. It is seen that these terms split the otherwise degenerate modes, but because of their small size relative to the exchange terms in NiO the splitting is only important near $q = 0$. The usual linear spin-wave theory will give the above expressions with $\eta = 1$. However Lines,[35] and others, have pointed out that careful consideration of the con-

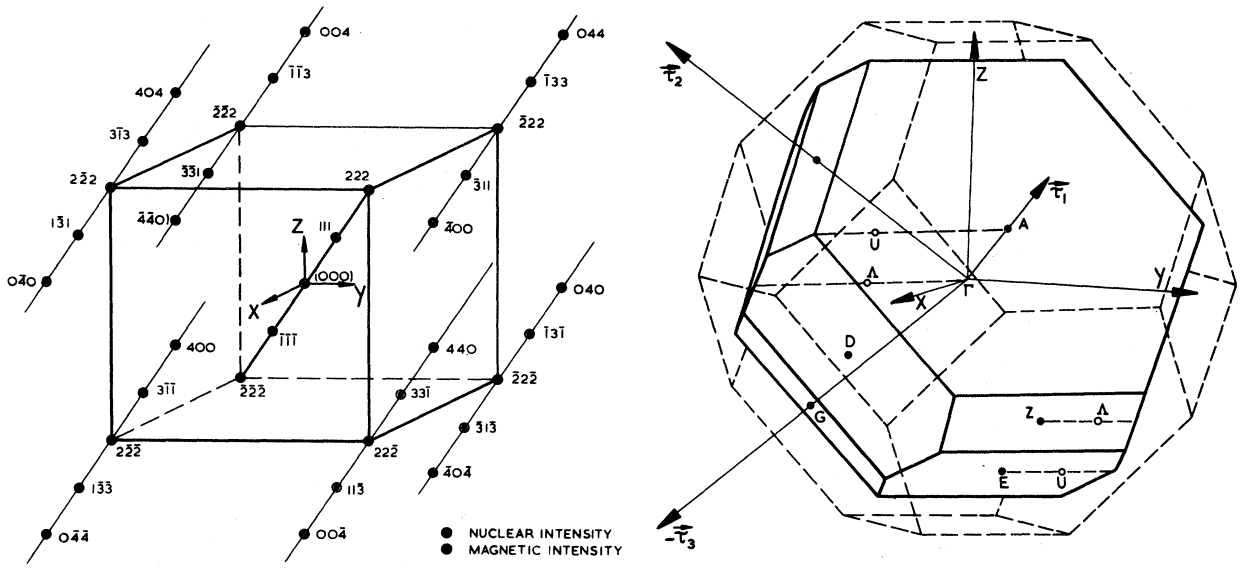

FIG. 2. Antiferromagnetic reciprocal lattice of domain A, and corresponding Brillouin zone (after Ref. 29). The paramagnetic zone is shown in dashed line.

ventionally higher-order terms in the deviation operations occurring in the anisotropy Hamiltonian can yield additional effectively linear contributions. For the case of NiF_2 plausibility arguments have been given which suggest η, the factor by which the terms in the energy derived on simple linear spin-wave theory must be multiplied, is given for the $(S_x^2 - S_y^2)$ and S_z^2 terms in the Hamiltonian by $\eta = (1 - \frac{1}{2}S) = \frac{1}{2}$.[36] By analogy we have assumed $\eta = \frac{1}{2}$ in our case too. Loudon[37] and Stevens[38] have recently considered the problem by treating the spin waves as excitations from the molecular field ground state. If $|J_2| \gg |J_1|$ they find expressions similar to Eqs. (2), with η set equal to $\frac{1}{2}$. However, their results differ from Eqs. (2) in that D_1 occurs in *both* brackets in the expression for $E_1(\vec{q})$, and D_2 in both for $E_2(\vec{q})$. If J_2 is not much greater than J_1 the relation is more complicated. In the case of NiO where, as we shall find, $|J_2| \gg |J_1|$ and J_2 is also very much larger than the anisotropy terms, we may use the relations given in Eqs. (2) since they are very close to the more exact expressions.

Random-phase-approximation Green's-function theory gives spin-wave energies similar to Eqs. (2) but with S replaced by $\langle S_z \rangle_T$.[2,39] As $\langle S_z \rangle_{T=0}$ is less than S this represents a reduction in energy for a given set of Hamiltonian parameters. However, it should be noted that other alternative theories, such as that of Oguchi which includes higher-order terms in the spin-wave operators (the dynamical interactions), give a factor which *increases* the energy by an amount of about the same order, that is by a few percent.[40]

The complete expansions of Eqs. (2) for the different domains are given in the Appendix. One particularly interesting feature is that the zone boundary energy of the spin waves may be very low in some directions. For example at the 111 point of a multidomain sample, where the [111] zone boundary point of domains B, C, and D, coincides with the zone center point of domain A, the zone boundary energies are only nonzero because of the finite values of $(J_1^+ - J_1^-)$, D_1, and D_2. We note also from symmetry considerations that for a multidomain sample the dispersion curves for the domains C and D will always coincide in the $(1\bar{1}0)$ plane, and in the [111] and $[11\bar{1}]$ directions they will furthermore coincide with those of domain B or A, respectively.

B. Neutron Scattering

The cross section for inelastic neutron scattering from a fluctuating spin system of N spins is given by[41]

TABLE II. Types of neighbors of an up spin (↑) in a domain of NiO. j is the neighbor index; z_j, the number of neighbors; J_j, their interaction parameter; and δ_j, their separation.

	Cubic		Rhombohedral		
j	z_j	J_j	z_j	δ_j	δ_j(Å) (~ 78 °K)
1	12	J_1^+	6↓	$a_0(1 - \frac{1}{2}\Delta)/\sqrt{2}$	2.948
		J_1^-	6↑	$a_0(1 + \frac{1}{2}\Delta)/\sqrt{2}$	2.952
2	6	J_2	6↓	a_0	4.17
3	24	J_3^+	12↓	$(\frac{3}{2})^{1/2} a_0$	5.11
		J_3^-	12↑		
4	12	J_4	12↑	$\sqrt{2}\, a_0$	5.90

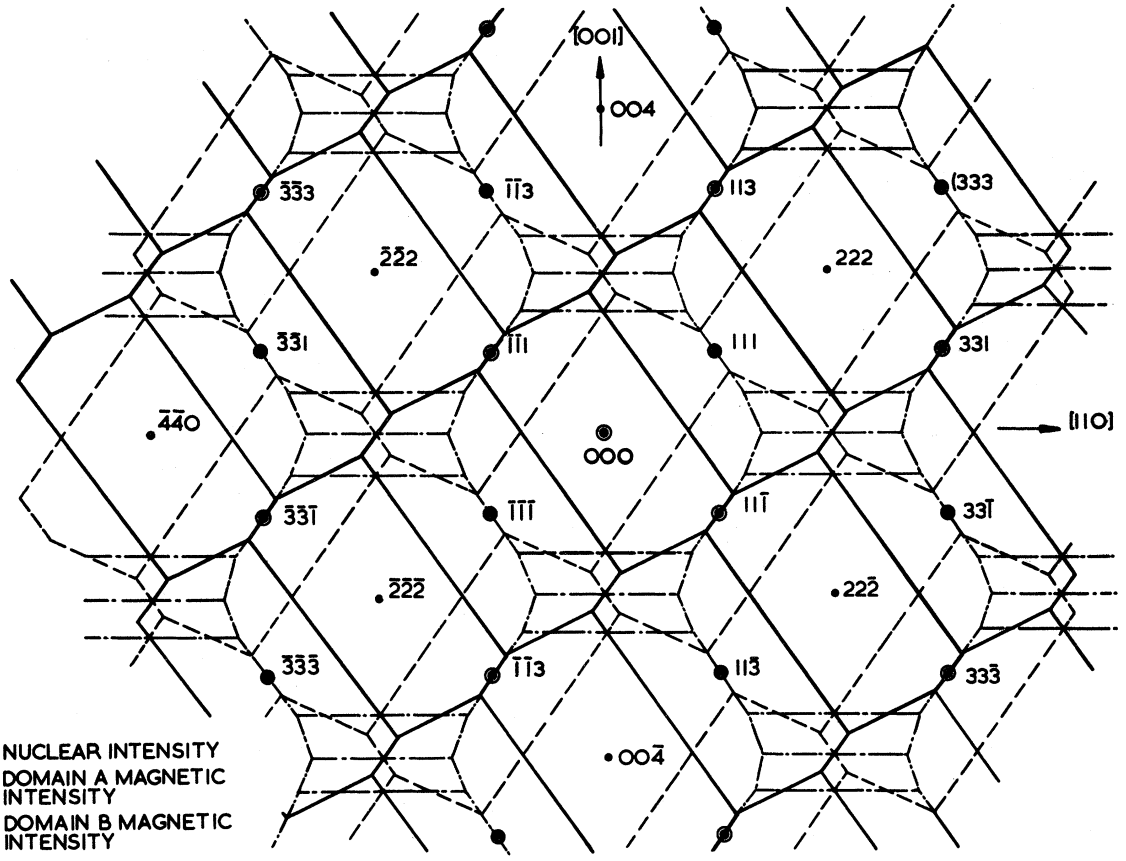

FIG. 3. $(1\bar{1}0)$ plane of the reciprocal lattice with zone boundaries of domain A (heavy lines), domain B (dashed lines), and domains C and D (dash-dotted lines).

$$\frac{d^2\sigma}{d\Omega' dE'} = A(\vec{k},\vec{k}')\sum_{\alpha\beta}(\delta_{\alpha\beta}-\hat{Q}_\alpha\hat{Q}_\beta)\mathcal{S}^{\alpha\beta}(\vec{Q},\omega) \quad , \tag{3}$$

where

$$A(\vec{k},\vec{k}')=\frac{N}{\hbar}(\gamma r_0)^2\frac{k'}{k}\,|f(\vec{Q})|^2, \quad r_0=\frac{e^2}{mc^2}$$

where e and m are the charge and mass of the electron, γ is the gyromagnetic ratio for the neutron, and $f(\vec{Q})$ is the neutron form factor. $\vec{k}, E$ and $\vec{k}', E'$ are the initial and final wave vector and energy of the neutron, respectively; $\vec{Q}=\vec{k}-\vec{k}'$ is the scattering vector; and $\hbar\omega = E - E'$ is the neutron energy change. $\hat{Q}$ denotes a unit vector, and the van Hove scattering function is defined by

$$\mathcal{S}^{\alpha\beta}(\vec{Q},\omega) = (1/2\pi)\int_{-\infty}^{\infty}\sum_{\vec{r}} e^{i(\vec{Q}\cdot\vec{r}-\omega t)}\langle S^\alpha(0)S^\beta(t)\rangle_T dt \quad . \tag{4}$$

For a simple two-sublattice antiferromagnet with the spin direction as $0z$, the cross section becomes[42]

$$\frac{d^2\sigma_{\pm}}{d\Omega' dE'} = A(\vec{k},\vec{k}')\tfrac{1}{2}S\,|M(\vec{q},\vec{\tau}_m)|^2(1+\hat{Q}_z^2)(n_{\vec{q}}+\tfrac{1}{2}\pm\tfrac{1}{2})$$
$$\times\,\delta(\hbar\omega - E_{\vec{q}})\delta(\vec{Q}-\vec{\tau}-\vec{q}) \quad . \tag{5}$$

Here $\vec{\tau}_m$ is a magnetic reciprocal-lattice vector and $\vec{q}$ is the wave vector of the excitation of energy $E_{\vec{q}}$ created (+) or destroyed (−). $M(\vec{q},\vec{\tau})$ is the dynamic structure factor, and if $\vec{\tau}_{mB}$ is a reciprocal-lattice point with finite static magnetic structure factor,

$$|M(\vec{q},\vec{\tau}_{mB})|^2 = (A_{\vec{q}}+B_{\vec{q}})/(A_{\vec{q}}^2-B_{\vec{q}}^2)^{1/2} \quad .$$

As the anisotropy is relatively small in NiO we may use these relations to calculate the scattering intensities; they should be very good approximations except near $\vec{q}=0$ when the anisotropy becomes important. Care must be taken in calculating the cross section for scattering from each domain at a particular point in the reciprocal lattice of a multidomain sample, as in the case of the spin-wave energies (see the Appendix). It is generally found that the intensity from all domains is highest near a point in reciprocal space where there is magnetic Bragg intensity from any one domain.

Because of the finite resolution of a three-axis spectrometer, the intensity observed at a setting to observe $(\vec{Q}_0,\omega_0)$ is given by

$$I(\vec{Q}_0, \omega_0) = \int\int R(\vec{Q} - \vec{Q}_0, \omega - \omega_0)\sigma(\vec{Q}, \omega)\, d\vec{Q}\, d\vec{\omega} \quad , \tag{6}$$

where $\sigma(\vec{Q}, \omega)$ is the scattering cross section [Eq. (3)] transformed to variables $\vec{Q}$ and ω, and R is the resolution function of the instrument.[43] The line shapes of the neutron groups may be calculated theoretically by performing this convolution on a computer, and adding the contribution from each domain. The program written by Samuelsen and Hutchings[44] was used extensively in the present work, as it was necessary to establish if scattering from the different domains could be distinguished, and to make the often large resolution corrections to the data.

IV. EXPERIMENTS

A. Sample

The sample used consisted of two carefully aligned crystals of total volume ~4 cm^3. The crystals were grown by the Marubeni-Iida Co. Ltd., Japan, using the Verneuil technique and are black in color. The Bragg peaks indicated a mosaic width of the order of 20′ and the two crystals were aligned to better than 5′ with their $[1\bar{1}0]$ directions vertical. The sample consisted of equally populated T domains, as judged from the intensities of the 111 M Bragg peaks. No splitting of the 222 N Bragg peak was seen indicating that any difference in orientation of the domains due to the rhombohedral distortion was unobservable. A brief attempt was made to create a single-domain crystal using the "anneal and pinch" technique of Slack.[21] However, it appeared that crystals as large as those required for neutron scattering would require very long annealing times at ~1500 °C for success, and as a suitable furnace was not available a multidomain sample was used for the experiments.

The sample was mounted in an aluminum can attached to the cold finger of a Cryogenic Associates CT14 cryostat. The sample temperature was maintained at 78 °K throughout the experiment.

B. Procedure

All the data presented in this paper were taken on the H7 and H8 triple-axis spectrometers at the Brookhaven high-flux-beam reactor using neutron energy loss. Some preliminary measurements were however made on the Dido triple-axis spectrometer and Pluto time-of-flight spectrometer at AERE Harwell, in collaboration with R. J. Birgeneau.

Because of the very high initial slope of the dispersion (~250 meV Å) most measurements of the lower part, with the exception of $q = 0$, were made with constant-E scans. By comparing the experimental line shape of the neutron groups with that calculated from Eq. (6) using approximate theoretical dispersion curves and a resolution function calculated from the known mosaics and collimator angles, the corrected value of the wave vector could be found. The simultaneous presence of excitations from each of the four domains gives rise to a further difficulty, but as we shall see the fact that J_1 is very much less than J_2 causes their energies to lie very close together. Indeed, the excitations from different domains were only clearly resolved at $q = 0$, and careful calculation of the line shapes confirmed that they were, in fact, unresolvable at higher energies. At the highest energies, measurements were made using constant-q scans.

The lower energy (< 60 meV) spin waves were measured using germanium (220) or (111) planes to monochromate the neutrons, and either pyrolytic graphite (002) or germanium (111) planes as analyzer. At higher energies, up to 200-meV incident neutron energy, beryllium (110) used in transmission was found to be the best choice for monochromator,[45] the scattering angles for the beryllium (002 reflection) becoming very small. The (002) plane of a large zinc crystal, or the (004) plane of pyrolytic graphite, was used in reflection as analyzer. The monochromated neutron intensity fell off rapidly with energy, necessitating count times of 20 min/point for the highest-energy spin waves. For example, if the incident intensity on the sample is taken as unity at 80 meV, it was 0.7 at 100 meV, 0.35 at 150 meV and 0.1 at 200 meV. Collimation angles were usually 20′ before the monochromator, 40′ before and after the sample, and either 20′ or 40′ before the counter. 20′ collimation throughout was used for some low-energy scans.

The spin waves were measured relative to magnetic reciprocal-lattice points $\vec{\tau}_m$ on both domains A and B. The lowest-energy spin waves were measured about the innermost 111 and $11\bar{1}$ points, but as the energy increased the 113 and $11\bar{3}$, and 331 and $33\bar{1}$ had to be used. Because of the variation of cross section with $|f(\vec{Q})|^2$ the use of larger scattering vectors causes a reduction in intensity. The lowest-energy measurements were made with the spectrometer in the W configuration, but calculations showed that the best focusing of the spin waves with higher energy could be obtained with the analyzer arm in the other sense, and this configuration was used for many of these measurements.

C. Experimental Data and Results

The energy dispersion was determined in five directions in reciprocal space. Referring all ex-

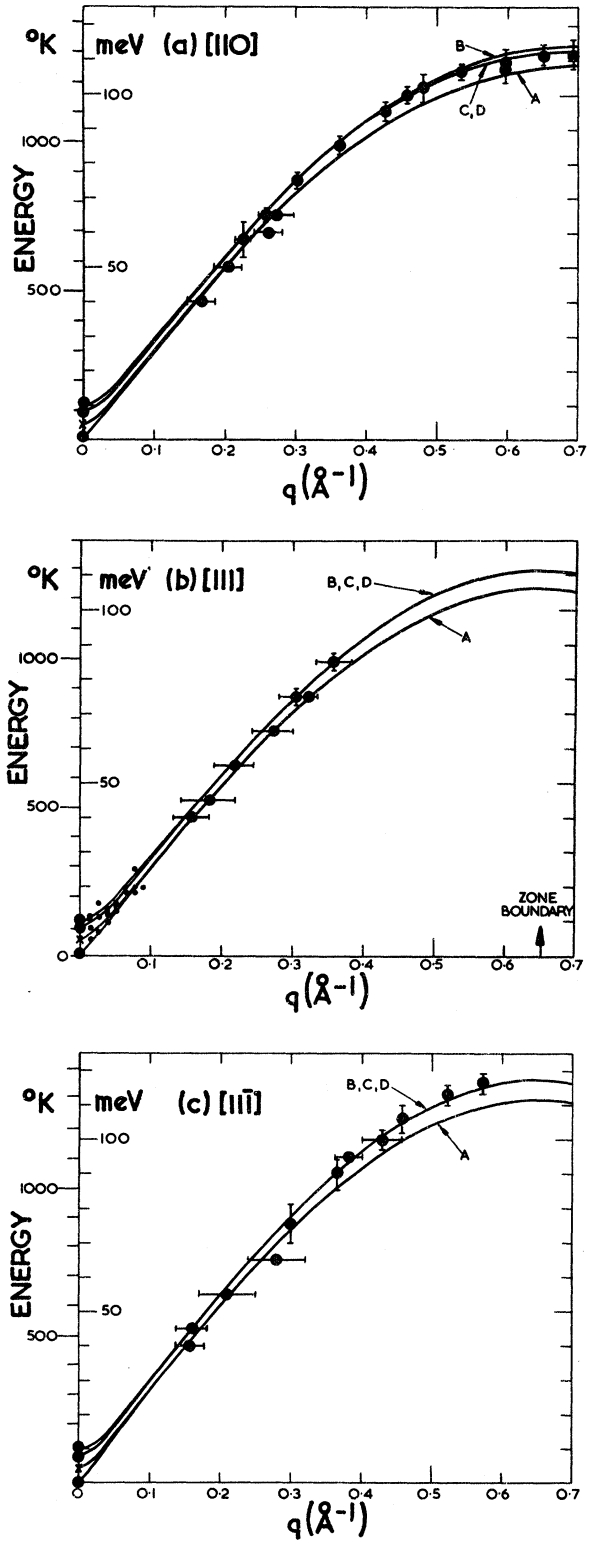

FIG. 4. Spin-wave dispersion in (a) [110], (b) [111], and (c) [11$\bar{1}$] directions. Wave vectors are given in Å^{-1}. The reciprocal-lattice vectors in these directions are $\tau_{110}=1.065$ Å^{-1} and $\tau_{111}=1.305$ Å^{-1}. The error bars represent 95% confidence limits.

citation wave vectors q to the 111 reciprocal-lattice point, these were [110], [001], [111], [11$\bar{1}$], and [11$\bar{3}$]. In referring the wave vectors measured about other reciprocal-lattice points back to the 111 point, one must of course take into account the orientation of the Brillouin zones of different domains. The data points in the [110], [111], and [11$\bar{1}$] directions corrected for small shifts due to resolution effects are plotted in Figs. 4(a)–4(c). The dispersion was found to be very similar in all directions, indicating a low value of J_1 relative to J_2, and in confirmation of this the excitations from different domains were generally not resolved at large wave vectors.

The intensity profile observed in a constant-q scan at 11$\bar{1}$ is shown in Fig. 5. There are two main neutron groups, the lower one corresponds to the zone center excitation of domain B, while the intensity at 8–12 meV is attributed to excitations in domains A, C, and D. The zone center modes correspond to the antiferromagnetic resonance (AFMR) modes. Only one of these has been observed by infrared techniques, that corresponding to a precession of spins out of the ordering plane involving the larger anisotropy D_1. Kondoh[13] and Sievers and Tinkham[46] find this to be at 4.54 meV (= 36.6 cm^{-1} = 52.7 °K). We do not observe this mode at 11$\bar{1}$ since the associated spin fluctuations lie wholly along the scattering vector $\vec{Q}$ and the term $(1-\hat{Q}_\alpha^2)$ in Eq. (3) for the cross section is then zero. A weak peak at ~4.5 meV was, in fact, seen at 33$\bar{1}$ and 11$\bar{3}$. We attribute the intensity peaking at 2 meV to the lower, in-plane, AFMR mode which involves D_2, and after correcting for instrumental resolution effects we find its excitation energy to be at 1.0 ± 0.5 meV (~8 cm^{-1} ~ 11°K). We identify the two upper peaks as the two zone boundary modes of domains A, C, and D. Their magnetic character was established by a falloff in their intensity with $\vec{Q}$ and their absence at nuclear points 22$\bar{2}$, 44$\bar{4}$, and at 220.

The solid line in Fig. 5 represents the calculated intensity found by convoluting the cross section given in Eq. (3) with the resolution function. It is seen that although there is not exact agreement in the energy of the upper group the general relative intensities of the two groups confirm their identity. To account for their detailed shape would necessitate the inclusion of additional terms in the Hamiltonian, and possibly the exact orientation of the different domains. It appears that there may well be a small contribution to the observed intensity from the mode at 4.5 meV allowed by the finite instrumental resolution.

Away from the reciprocal-lattice points the separate modes rapidly become indistinguishable as they rise in energy, and the excitations from the different domains come closer in energy. This is

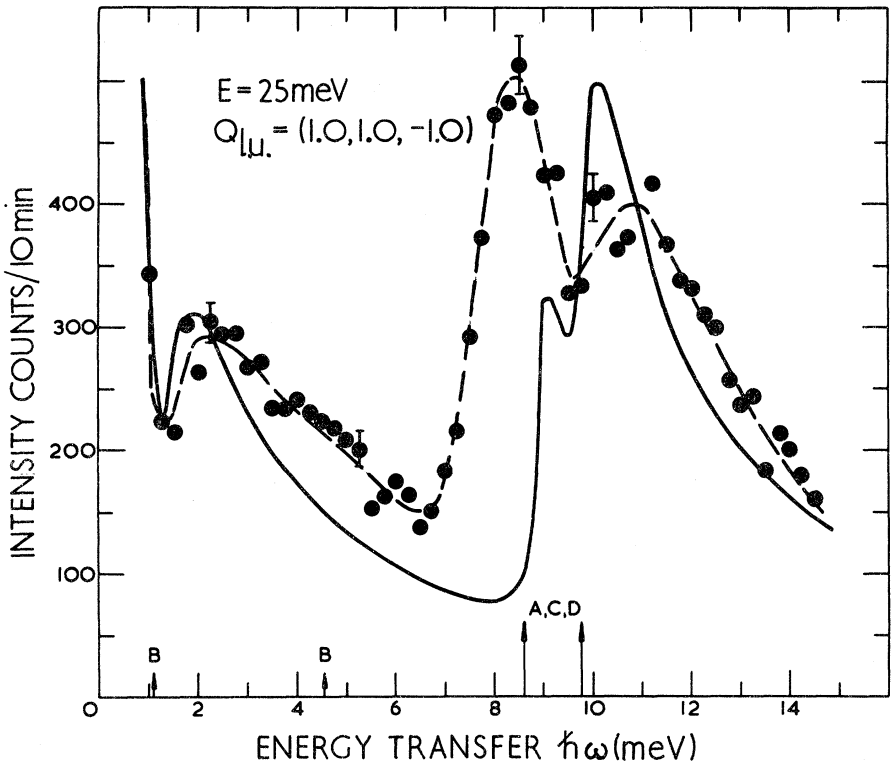

FIG. 5. Intensity observed at $11\bar{1}$. The dashed line is experimental; the solid line is calculated from Eq. (6) normalized at the highest point and the background.

seen from the lower-energy points in Fig. 4(b) represented by small dots, which are uncorrected for resolution effects. Once the two spin-wave modes from each domain have become virtually degenerate we would expect Eq. (5) to describe the cross section very well. Four typical convolutions of the resolution function and the cross section using the best-fit parameters are shown in Fig. 6. It is seen that the line shapes are well accounted for, although there is a slight shift in energy in some peaks due to the inaccuracies in the fitted spin-Hamiltonian parameters. It is clear from Fig. 6 that the excitations from different domains cannot be resolved.

D. Fitting to Data

The spin-Hamiltonian parameters were determined by fitting Eqs. (2) to the data using a generalized-least-squares routine. The neutron groups were first identified with a particular domain or average of domains, and fits made to the uncorrected wave vector and energies of the peak intensities. Convolutions of the cross section calculated using the approximate parameters and resolution were then made to find the corrections to the peak positions, and finally fits were made to the corrected data. Each point was weighted according to the error in both $\vec{q}$ and $\vec{E}$. In all the fits the upper AFMR mode frequency was set to 4.54 (± 0.04) meV, as found from infrared measurements.[13,46]

Several fits with different numbers of variables were made, but in general the inclusion of exchange parameters more distant than first and second neighbors leads to high correlations between the parameters, and only slightly reduces the "goodness of fit" parameter χ_F. The results of these fits are listed in Table III. We regard the values given in the top line as adequately representing the data, and have used these for the calculation of magnetic properties. Although there are large errors on the individual magnitudes of J_1^+ and J_1^- their difference $J_1^+ - J_1^- = (0.45 \pm 0.20)$ °K is determined much more accurately. The errors given in the table include estimates of contributions from all sources and represent 95% confidence limits.

V. DISCUSSION OF RESULTS

A. Exchange and Anisotropy Parameters

The most striking feature of the exchange interactions in NiO listed in Table III is the much smaller magnitude of the nn exchange J_1 compared with that between nnn J_2. As we see below, this is in accord with simple ideas of exchange involving effects of covalency and electron overlap. Previous experimental estimates of the magnitude of the interactions have been made from the transition temperature and the susceptibility measurements of Singer.[47] Typical results from these data are compared with the present values in Table IV.

TABLE III. Values of spin-Hamiltonian parameters of Eq. (1), in °K, obtained by several fits of Eq. (2) to the spin-wave data at 78 °K. N_p is the number of parameters fitted. χ_F is the mean of the square of the ratio of the deviation from the calculated value of the energy of each fitted point to its experimental uncertainty.

N_p	D_1	D_2	J_1^+	J_1^-	$J_1^+ - J_1^-$	J_2	J_3	J_4	χ_F
3	1.13	0.06[a]	−15.7	−16.1	0.45	221	...	...	0.29
	(±0.04)	(±0.05)	(− 6.0) (+ 10.0)	(− 6.0) (+ 10.0)	(±0.20)	(±4)			
3	1.24	0.06[a]	−23.3	−23.8	0.43	221[a]	−5.2	...	0.27
	(±0.04)	(±0.05)	(−8.0) (+ 18.0)	(− 8.0) (+ 18.0)	(±0.20)		(±4.0)		
4	1.04	0.06[a]	−14.7	−15.1	0.40	245[b]	...	11.0[b]	0.34
	(±0.06)	(±0.05)	(− 8.0) (+10.0)	(− 8.0) (+10.0)	(±0.20)	(±14)		(+6.0)	
5	1.13	0.06[a]	−22.4	−22.7	0.40	238[b]	−6.4	8.3[b]	0.22
	(±0.06)	(±0.05)	(−10.0) (+18.0)	(−10.0) (+18.0)	(±0.20)	(±14)	(±7.0)	(±5.3)	

[a]Held fixed.

[b]Highly correlated.

Whereas they give J_2 of the correct order of magnitude, they tend to give large antiferromagnetic values for J_1. The reason probably lies in the fact that the paramagnetic Curie temperature θ is not well determined in Singer's measurements, which only go up to $T \sim 2.5\, T_N$, and in the uncertainty in interpreting his data to obtain accurate values for the susceptibility $\chi(T_N)$ or $\chi_\perp(0)$. We shall see below that values of these quantities calculated from our parameters are in some disagreement with the experimental data. The recent Raman scattering data are, however, in accord with our results. Dietz *et al.*[16] also find J_1 is small; their value for J_2, in fact, assumes J_1 to be zero.

The nn and nnn Ni^{2+} ions in NiO are linked by 90° and 180° superexchange paths involving one intervening O^{2-} anion. They are therefore particularly amenable to theory, and have been the subject of several theoretical treatments.[48] The basic ideas are reviewed by Owen and Thornley,[1] and a quantitative estimate of J_2 has been made by Anderson.[48,49] The nnn interaction is attributed to bonding of the Ni^{2+} $(3d)^8$ e_g (strong-field approximation) orbitals with the O^{2-} p_σ orbital. J_2 is shown to be proportional to the square of the spin transfer coefficient f_σ, and is given roughly by $J_2 \approx \frac{1}{9}\Delta_c^2/U$, where Δ_c is the single-electron crystal field splitting and U the energy required to transfer an electron from one Ni^{2+} ion to another. Using values of $\Delta_c = 12\,240$ °K and $U = 73\,000$ °K, J_2 is predicted to be 230 °K, in remarkably close agreement with the experimental value. The interaction is antiferromagnetic in sign since the unpaired spin is transferred into the same p_σ orbital from both Ni^{2+} ions, and the two spins align antiparallel by the Pauli exclusion principle. In the case of the nn 90° bond, the π-bonding mechanism proposed by Casselman and Keffer[50] for MnO is inoperative for the Ni^{2+} e_g orbitals. There will be an antiferromagnetic contribution proportional to f_s^2 and a ferromagnetic contribution proportional to f_σ^2, but no unambiguous quantitative estimate has been made of the relative size of these contributions. In NiO $f_\sigma^2 \gg f_s^2$ so that we expect the antiferromagnetic contribution to the nn interaction to be much smaller than that to the nnn interaction. The fact that we observe a small ferromagnetic nn interaction suggests that the ferromagnetic contribution is the largest. However there could also be a ferromagnetic contribution from direct exchange.[48]

The small difference between J_1^+ and J_1^- may be related to the measured lattice contraction. Following Lines[4] we define j by $(J_1^+ - J_1^-) = 2j\langle S_z\rangle^2$, and from the measured value of $(J_1^+ - J_1^-) = (0.45 \pm 0.20)$ °K we find $j = (0.26 \pm 0.13)$ °K. j may be expressed in terms of the distortion angle Δ, and the variation of exchange with separation $\epsilon_1 = -(r/J_1) \times \partial J_1/\partial r$ by $j = J_1 \epsilon_1 \Delta / 2\langle S_z^2\rangle$. Bartel and Morosin[14,51,52] summarize the exchange striction relations, and express $J_1\epsilon_1$ in terms of Δ and the elastic constant c_{44}. Using their measured value of $\Delta = 4.5'$ and a value of c_{44} scaled from that of MnO, we calculate $j = 0.15$ °K. If Slack's[21] value of $\Delta = 6'$ is used we find $j = 0.27$ °K. The agreement with the experimental value is quite satisfactory. We may note that since j is positive and J_1 is ferromagnetic (negative), ϵ_1 is negative and $\partial J_1/\partial r$ is a positive quantity.

Previous determinations of the anisotropy have been mainly confined to the out-of-plane constant K_1, where K_1 is usually related to our parameter

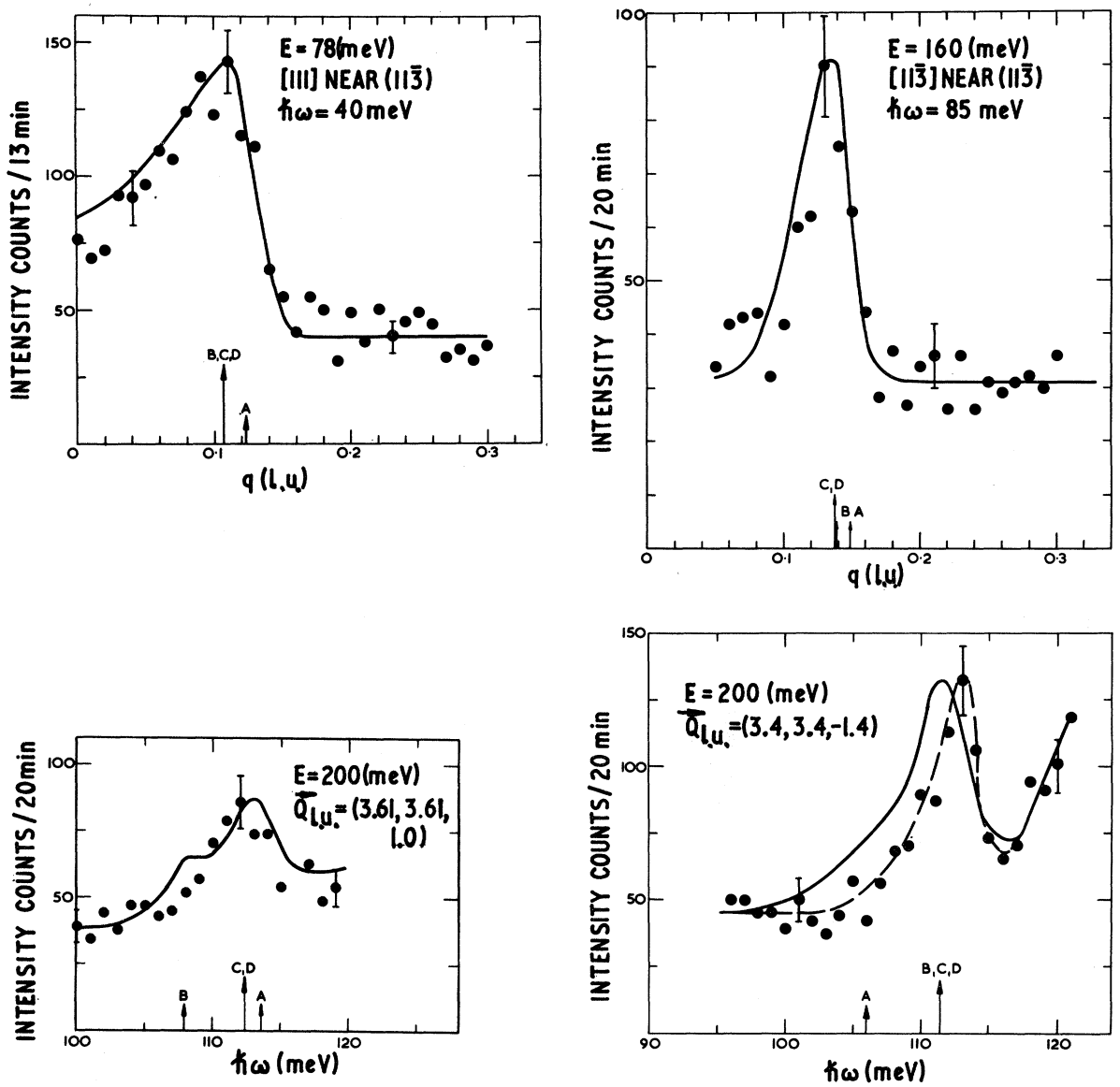

FIG. 6. Intensity observed in four typical scans. The wave vectors in the two constant-q scans are expressed in lattice units (l. u.) $\tau_{111}=1.305$ Å^{-1} and $\tau_{11\bar{3}}=2.498$ Å^{-1}. The arrows indicate the calculated position of the excitations in the four domains. The solid lines are calculated from Eq. (6) and are normalized to the peak and background levels.

D_1 by $3K_1/NS^2=D_1$. Here N is the number of Ni^{2+} ions/cm^3, and K_1 is in erg/cm^3. The value of K_1 has been determined from the upper AFMR frequency, $\hbar\omega_1=52.7\ ^\circ\mathrm{K}=g\mu_B[3K_1/\chi_\perp(0)]^{1/2}$, and therefore is subject to the errors discussed above arising from the uncertainty in value of $\chi_\perp(0)$ adopted. Kondoh[13] used $\chi_\perp(0)=11.8\times10^{-6}$ emu/g, and found $K_1=3.32\times10^6$ erg/cm^3 giving $D_1=1.31$ °K, slightly larger than our value of 1.13 °K. Kaplan[31] has calculated the contribution to K_1 from dipolar interactions alone and finds D_1 (dipolar) = 1.8 °K. This is somewhat higher than the experimental values and suggests a negative contribution arising from other sources such as the single-ion anisotropy.

There have been a few previous estimates of the in-plane anisotropy made from both torque measurements[10,28,53] and from theory.[26] These indicate that this anisotropy may be sample dependent and suggest that its magnitude is $\sim10^{-3}$ of that of the out-of-plane anisotropy. This is considerably lower than suggested by our value of $D_2\sim0.06$ °K determined from the lowest zero-wave-vector excitation. It should be relatively

TABLE IV. Comparison of present values for the spin-Hamiltonian parameters with the results of previous work and theoretical estimates (°K).

Experiment	D_1	D_2	J_1^+	J_1^-	J_2
Present neutron work	1.13 (±0.04)	0.06 (±0.05)	−15.7 (− 6.0) (+10.0)	−16.1 (− 6.0) (+10.0)	221 (±4)
Molecular field theory[a] from θ and T_N	...	...	100		170
Green's-function theory[b] from T_N and χ			~150 (±25)		~216 (±35)
Raman scattering[c]			small		213 (±2)
AFMR, $\chi_\perp(0)$[d]	1.31				
Theory					
Dipolar[e]	1.8				
Superexchange[f]			small		230

[a]Reference 12. [d]Reference 13.
[b]Reference 14. [e]Reference 31.
[c]Reference 16. [f]References 49 and 1.

easy to resolve this discrepancy using present day far-infrared or microwave techniques to check the lowest AFMR mode.

B. Calculation of Magnetic Properties

1. Density of States

The density of spin-wave states was calculated using the best-fit parameters and is shown as the solid line in Fig. 7. To indicate the effect of the nn interactions, the density of states is also shown calculated with only a nnn interaction J_2 = 221 °K present. The calculations were made by sampling energies at 270000 points evenly distributed in q space over the irreducible $\frac{1}{12}$th section of the antiferromagnetic Brillouin zone shown in Fig. 2. It can be seen from Fig. 7 that the presence of the small nn interaction pushes the cutoff in the density to higher energies and may help to account for the high-energy tail observed in the Raman scattering.[16] However the maximum energy at 119 meV is still a little higher than that suggested by the Raman data, 116.5 meV.

It is interesting to note that the recently observed tunneling characteristics of Ni-NiO-metal junctions measured by Adler and Chen[54] show a broad peak in the derivative of the even part of the conductance in the region 100–110 meV. It seems quite possible that this arises through an additional tunneling channel opening up at this voltage which involves inelastic scattering of the tunneling electrons from magnons, as the peak is close to that at 112 meV in the density of states. This suggestion has been confirmed during the preparation of this paper by further experiments by Tsui *et al.*[55]

2. Sublattice Magnetization

The temperature variation of the sublattice magnetization and other magnetic properties have been determined from the RPA Green's-function relations given by Lines[2,3] and by Mills *et al.*,[39] by performing the appropriate summations over the irreducible unit of the Brillouin zone. In all these calculations the best-fit parameters given in the top line of Table III were used, although the other sets of parameters give the same results since they reproduce the dispersion relations and density of states very closely.

The temperature variation of the sublattice magnetization is shown in Fig. 8. RPA theory gives a variation which is quite close to that given by molecular field theory; for comparison both have been normalized to a value of $\langle S_z\rangle_{T=0} = 0.924$ and the strict RPA $T_N = 648$ °K discussed in Sec. V B 3. The experimental points plotted in Fig. 8 are those of Roth.[9] They show a much slower falloff of $\langle S_z\rangle_T$ with T/T_N than given by theory, in a manner very reminiscent of MnO. However, it appears that the cause for this difference cannot be attributed to exchange striction in this case, since the approximation we have used in the theoretical calculations, that $(J_1^+ - J_1^-)$ is temperature independent, seems fully justified. This is because both the magnitude of the distortion and the value of spin, and hence $(J_1^+ - J_1^-)$, are much smaller in NiO than in MnO. In fact we find $j/J_2 = 0.0014$, and from the work of Lines and Jones[4] and of Bar-

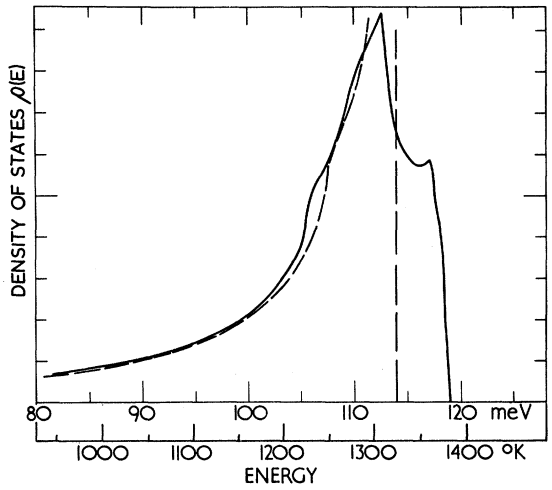

FIG. 7. Density of spin-wave states in NiO. Solid line is calculated from the best-fit parameters, Table III, and dashed line from $J_2 = 221$ °K alone.

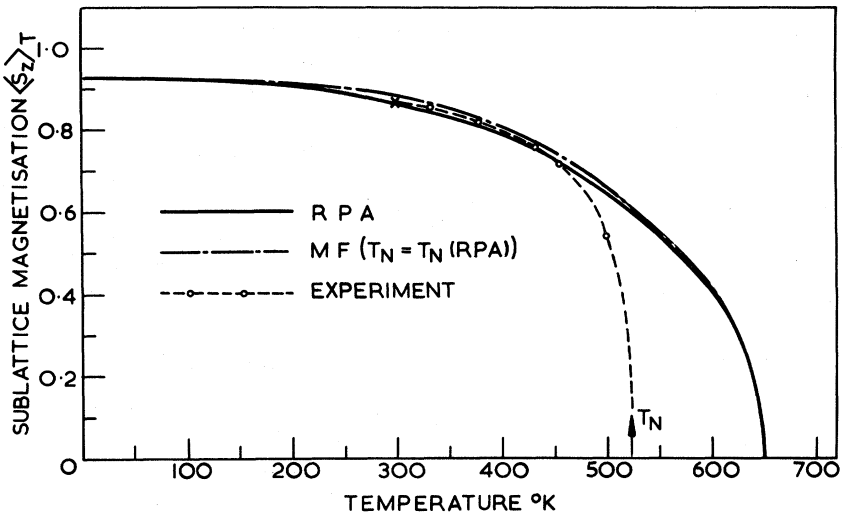

FIG. 8. Temperature variation of the sublattice magnetization. Molecular field theoretical variation has been normalized to RPA results at 0 °K and $T = T_N$. The experimental points (Ref. 9) are normalized to the RPA theory at 297 °K.

tel and Morosin[14] this would appear to have very little effect on the variation of $\langle S_z \rangle_T$. The discrepancy with experiment is therefore surprising, but it is felt that the experimental sublattice magnetization variation should be checked before further theoretical work, such as the possible attribution of the difference to biquadratic exchange, is pursued.

The value calculated for $\langle S_z \rangle_{T=0}$ is less than $S=1$, the molecular field value, because of the zero-point deviation. We find $\langle S_z \rangle_{T=0} = 0.9242 \pm 0.0003$, close to the value of 0.922 predicted by spin-wave theory for a simple cubic antiferromagnet. This reflects the small value of J_1, and the type-II magnetic order which for vanishing J_1 may be considered as four interpenetrating unconnected simple cubic lattices. Measurements of $\langle S_z \rangle$ by neutron diffraction yield a value less than 0.924 because of covalency effects,[56] and have been used to determine covalency parameters in NiO which are difficult to obtain from more conventional spin resonance experiments. Both Alperin[57] and Fender *et al.*[58] have measured $\langle S_z \rangle$ at low temperatures and find a value of 0.82, with errors of ~10 and ~1%, respectively, which perhaps overestimate and underestimate the true error. Fender *et al.* use the simple cubic zero-point deviation to obtain the spin transfer parameters. Our calculated deviation confirms their results, namely, that $(f_\sigma + f_s) = 3.8\%$. This is quite close to the values ~3.7–4.3% found from NMR in $KNiF_3$.

3. *Néel Temperature and Susceptibility*

In Table V we summarize a number of other magnetic properties calculated using molecular field theory and RPA Green's-function theory,[2,3,39] and compare them with the experimental values.

The molecular field value of 886 °K overestimates T_N as is usual. The value given by RPA, 648 °K, is that calculated using spin-Hamiltonian parameters derived from the RPA expression for the spin-wave energies, that is values which are greater than those given in Table III by $S/\langle S_z \rangle_{T=0}$. The same value is also obtained from an extrap-

TABLE V. Comparison of magnetic properties calculated from the fitted parameters using molecular field (MF) and RPA Green's-function theory with measured values.

Property	Calculated MF	Calculated RPA	Expt.
θ(°K)	−757 (−96) (+32)	−757 (−96) (+32)	−2000[a]
C_1(°K)	−1135 (−140) (+48)	−1135 (−140) (+48)	...
C_2(°K^2)	6.45×10^5 ($\pm1.6\times10^5$)	9.93×10^5 ($\pm2.4\times10^5$)	...
T_N(°K)	886 (±18)	648 (±10)	523[b]
$\chi(T_N)\times10^6$ (emu/g)	10.1 (±0.6)	10.1 (±0.6)	11.7[a] (±?)
$\chi_\perp(0)\times10^6$ (emu/g)	10.1 (±0.6)	8.9 (±0.5)	10.7[a] (±?)
$\langle S_z \rangle_{T=0}$	1.0	0.9242 (±0.0003)	0.82[c] (±~0.04)

[a]Reference 47.
[b]Reference 6.
[c]References 57 and 58 (includes covalency reduction ~11%).

olation of the $\langle S_z \rangle_T$-vs-T curves. If one uses the parameters given in Table III directly in the RPA formula one obtains $T_N = 601\,^\circ\mathrm{K}$, and if we decrease the parameters by an amount corresponding to the Oguchi correction for a simple cubic lattice,[40] that is by $1/(1+0.049)$, we obtain $572\,^\circ\mathrm{K}$. These latter two values, although from hybrid theories, are closer to the experimental value of $523\,^\circ\mathrm{K}$, but still lie above it. The RPA thus appears to be a better approximation than molecular field theory in NiO, but still overestimates T_N. This is in contrast to the calculations of Lines and Jones[4] for the $S=\frac{5}{2}$ case, where it is found that the RPA value of T_N is likely to be 5–10% too low, and to the results for Cr_2O_3,[43] and α-Fe_2O_3,[59] where the agreement is within a few percent.

From our results we calculate $\theta = -757\,^\circ\mathrm{K}$, much less than Singer's experimental value of $-2000\,^\circ\mathrm{K}$.[47] In Table V we also give values for the constants C_1 and C_2, the first two terms in the high-temperature expansion of χ,

$$\chi = (Ng^2\mu_B^2/\tau)(1 + C_1/\tau + C_2/\tau^2 + \cdots) ,$$

where $\tau = 3kT/S(S+1)$. These are given in molecular field theory[60] by

$$C_1 = 3k\theta/S(S+1) = -(6J_1^+ + 6J_1^- + 6J_2) \quad \text{and} \quad C_2 = \tfrac{1}{2}C_1^2 .$$

In RPA theory[4]

$$C_2 = 6(22J_1^2 + 24J_1J_2 + 5J_2^2) . \tag{7}$$

The RPA and molecular field theory give the same expressions for $\chi(T_N)$, that is

$$\chi(T_N) = Ng^2\mu_B^2/(12J_1^+ + 12J_2) . \tag{8}$$

Using $N = 5.51\times10^{22}/\mathrm{cm}^3$, $\rho = 6.832\ \mathrm{g/cm}^3$, and $g = 2.23$,[61] we calculate $\chi(T_N) = 10.1\times10^{-6}$ emu/g. Molecular field theory gives $\chi_\perp$ constant below T_N, but RPA[3,4] predicts a decrease to $\chi_\perp(0) = \chi(T_N)/(1+\Delta_1)$, where $\Delta_1 \sim 0.13/\langle S_z \rangle_{T=0}$. In our case $(1+\Delta_1) \sim 1.14$ and $\chi_\perp(0) = 8.89\times10^{-6}$ emu/g. Both $\chi(T_N)$ and $\chi_\perp(0)$ are some 15–20% lower than the experimental values we deduce directly from Singer's single-crystal data, using the known spin directions and assuming his sample to be single domain. This discrepancy appears to be well outside the errors expected. However, the interpretation of Singer's data may well be incorrect, indeed different authors have quoted differing values for $\chi_\perp(0)$ from the same data. Furthermore, it appears that no corrections have been made to the experimental susceptibility data for the Van Vleck temperature-independent contribution or for a diamagnetic contribution. We estimate that these amount to $(3.0\pm0.8)\times10^{-6}$ emu/g, and would thus reduce the uncorrected experimental values of $\chi(T_N)$ and $\chi_\perp(0)$ given in Table V by this amount. The corrected values should then correspond to the true ground-state susceptibility calculated by the theory we have used. In fact they now fall below the calculated values, possibly because the sample used for the measurements was not wholly single domain. It would, therefore, be advisable to await new measurements of the susceptibility, made with the more sensitive techniques and possibly purer, wholly single domain crystals now available, before attaching too much importance to the discrepancies.

VI. SUMMARY AND CONCLUSIONS

The spin-wave dispersion relations in fcc NiO have been measured at $78\,^\circ\mathrm{K}$, and from them values obtained for the main parameters in the spin Hamiltonian. The large antiferromagnetic nnn exchange interaction is found to predominate, and contrary to estimates previously made, the nn interaction is small and ferromagnetic. These findings are consistent with simple covalency and overlap theory for exchange interactions, confirming the picture of NiO as a weakly covalent insulator. There is a small difference between the interaction of parallel and antiparallel nn ion pairs in the ordered state and this difference is of the correct order of magnitude to be associated with the rhombohedral distortion of the crystal below T_N. We find the lower AFMR mode to be at $\sim 8\ \mathrm{cm}^{-1}$, and this should be easy to confirm by present day infrared techniques.

The density of spin-wave states in NiO has been calculated. It furnishes an explanation for a peak recently observed in the tunnelling characteristics of Ni-NiO-metal junctions. Magnetic properties have also been calculated using the spin-Hamiltonian parameters. The calculated sublattice magnetization curves and the susceptibilities are not in good agreement with measurement, but it is felt that at least part of these discrepancies may be due to poor experimental data.

ACKNOWLEDGMENTS

We wish to acknowledge the advice of G. Shirane in connection with the triple-axis measurements, and we are grateful to R. J. Birgeneau, W. J. L. Buyers, M. F. Collins, M. E. Lines, R. Loudon, and J. Owen for a number of helpful discussions.

APPENDIX

Including exchange interactions out to fourth neighbors and taking $S=1$ the energies of the two spin-wave modes of a single domain are given by

$$E_1^2(\vec{q}) = (A_{\vec{q}} - B_{\vec{q}} + D_1)(A_{\vec{q}} + B_{\vec{q}} + D_2) ,$$

$$E_2^2(\vec{q}) = (A_{\vec{q}} - B_{\vec{q}} + D_2)(A_{\vec{q}} + B_{\vec{q}} + D_1) ,$$

with

$$A_{\vec{q}} = (6J_2 + 6J_1^{+} - 6J_1^{-} - 12J_4 + 2J_1^{-}C_1 + 2J_3C_4 + 2J_4C_6) ,$$

$$B_{\vec{q}} = (2J_2C_2 + 2J_1^{+}C_3 + 2J_3C_5) .$$

For a domain of type A the terms C_n are

$$C_1 = \cos[\tfrac{1}{2}a_0(q_x - q_y)] + \cos[\tfrac{1}{2}a_0(q_y - q_z)] + \cos[\tfrac{1}{2}a_0(q_z - q_x)] ,$$

$$C_2 = \cos(a_0q_x) + \cos(a_0q_y) + \cos(a_0q_z) ,$$

$$C_3 = \cos[\tfrac{1}{2}a_0(q_x + q_y)] + \cos[\tfrac{1}{2}a_0(q_y + q_z)] + \cos[\tfrac{1}{2}a_0(q_z + q_x)] ,$$

$$C_4 = 2\{\cos[\tfrac{1}{2}a_0(q_y + q_z)]\cos(a_0q_x) + \cos[\tfrac{1}{2}a_0(q_z + q_x)]\cos(a_0q_y) + \cos[\tfrac{1}{2}a_0(q_x + q_y)]\cos(a_0q_z)\} ,$$

$$C_5 = 2\{\cos[\tfrac{1}{2}a_0(q_y - q_z)]\cos(a_0q_x) + \cos[\tfrac{1}{2}a_0(q_z - q_x)]\cos(a_0q_y) + \cos[\tfrac{1}{2}a_0(q_x - q_y)]\cos(a_0q_z)\} ,$$

$$C_6 = 2[\cos(a_0q_x)\cos(a_0q_y) + \cos(a_0q_y)\cos(a_0q_z) + \cos(a_0q_z)\cos(a_0q_x)] .$$

For domains B, C, and D we simply change the signs of q_z, q_y, or q_x, respectively, in the above formulas. In each case $\vec{q}$ is referred to a reciprocal-lattice point of the domain type under consideration.

---

*Work performed under the auspices of the U. S. AEC.

†Present address.

‡Guest Scientist from Institutt for Atomenergi, Kjeller, Norway (now returned).

[1]J. Owen and J. H. M. Thornley, Rept. Progr. Phys. 29, 675 (1966).

[2]M. E. Lines, Phys. Rev. 135, A1336 (1964).

[3]M. E. Lines, Phys. Rev. 139, A1304 (1965).

[4]M. E. Lines and E. D. Jones, Phys. Rev. 139, A1313 (1965).

[5]M. E. Lines and E. D. Jones, Phys. Rev. 141, 525 (1966).

[6]M. Foex, Compt. Rend. 227, 193 (1948); J. R. Tomlinson, L. Domash, R. G. Hay, and C. W. Montgomery, J. Am. Chem. Soc. 77, 909 (1955).

[7]C. G. Shull, W. A. Strauser, and E. O. Wollan, Phys. Rev. 83, 333 (1951).

[8]W. L. Roth, Phys. Rev. 110, 1333 (1958).

[9]W. L. Roth, Phys. Rev. 111, 772 (1958).

[10]W. L. Roth and G. A. Slack, J. Appl. Phys. 31, 352S (1960).

[11]See, for example, D. Adler, Solid State Phys. 21, 1 (1968); and L. F. Matheiss, Phys. Rev. B 5, 290 (1972); 5, 306 (1972).

[12]J. Smart, in *Magnetism*, edited by T. Rado and H. Suhl (Academic, New York, 1963), Vol. III, p. 97.

[13]H. Kondoh, J. Phys. Soc. Japan 15, 1970 (1960).

[14]L. C. Bartel and B. Morosin, Phys. Rev. B 3, 1039 (1971).

[15]The principal results of the present neutron work have been briefly reported by M. T. Hutchings and E. J. Samuelsen, Solid State Commun. 9, 1011 (1971); Bull. Am. Phys. Soc. 15, 337 (1970).

[16]R. E. Dietz, G. I. Parisot, and A. E. Meixner, Phys. Rev. B 4, 2302 (1971).

[17]M. Bonfante, B. Hennion, F. Moussa, and G. Pepy, Solid State Commun. 10, 533 (1972); in *Proceedings of Symposium on Neutron Inelastic Scattering, Grenoble*, 1972 (IAEA, Vienna, to be published).

[18]M. F. Collins, V. K. Tondon, and W. J. L. Buyers (private communication).

[19]J. Sakurai, W. J. L. Buyers, R. A. Cowley, and G. Dolling, Phys. Rev. 167, 510 (1968).

[20]H. P. Rooksby, Acta Cryst. 1, 226 (1948); N. C. Tombs and H. P. Rooksby, Nature 165, 442 (1950).

[21]G. A. Slack, J. Appl. Phys. 31, 1571 (1960).

[22]D. S. Rodbell and J. Owen, J. Appl. Phys. 35, 1002 (1964).

[23]H. Kondoh, E. Uchida, Y. Nakazumi, and T. Nagamiya, J. Phys. Soc. Japan 13, 579 (1958).

[24]W. L. Roth, J. Appl. Phys. 31, 2000 (1960).

[25]H. Kondoh and T. Takeda, J. Phys. Soc. Japan 19, 2041 (1964).

[26]T. Yamada, J. Phys. Soc. Japan 21, 650 (1966); 21, 664 (1966).

[27]T. Yamada, S. Saito, and Y. Shimomura, J. Phys. Soc. Japan 21, 672 (1966).

[28]E. Uchida, N. Fukuoka, H. Kondoh, T. Takeda, Y. Nakazumi, and T. Nagamiya, J. Phys. Soc. Japan 23, 1197 (1967).

[29]M. R. Daniel and A. P. Cracknell, Phys. Rev. 177, 932 (1969).

[30]J. S. Griffith, *The Theory of Transition Metal Ions* (Cambridge U. P., Cambridge, England, 1961), p. 191.

[31]J. I. Kaplan, J. Chem. Phys. 22, 1709 (1954).

[32]F. Keffer and W. O'Sullivan, Phys. Rev. 108, 637 (1957).

[33]J. M. Ziman, Proc. Phys. Soc. (London) 65, 540 (1952).

[34]See F. Keffer, in *Encyclopaedia of Physics* (Springer-Verlag, Berlin, 1966), Vol. XVIII/2, p. 1.

[35]M. E. Lines, Phys. Rev. 156, 534 (1967).

[36]M. T. Hutchings, M. F. Thorpe, R. J. Birgeneau, P. A. Fleury, and H. J. Guggenheim, Phys. Rev. B 2, 1362 (1970).

[37]R. Loudon (private communication).

[38]A. Stevens (private communication).

[39]R. E. Mills, R. P. Kenan, and F. J. Milford, Phys. Rev. 145, 704 (1966).

[40]T. Oguchi, Phys. Rev. 117, 117 (1960).

[41]W. Marshall and R. D. Lowde, Rept. Progr. Phys. 31, 705 (1968).

[42]O. Nagai and A. Yoshimori, Progr. Theoret. Phys. (Kyoto) 25, 595 (1961).

[43]M. J. Cooper and R. Nathans, Acta Cryst. 23, 357 (1967).

[44]See E. J. Samuelsen, M. T. Hutchings, and G. Shirane, Physica 48, 13 (1970); E. J. Samuelsen, in *Proceedings of the NATO Advanced Study Institute, Geilo, Norway*, 1971, edited by E. J. Samuelsen, E.

Andersen, and J. Feder (Universitetsforlaget, Oslo, 1971), p. 189.
[45]M. T. Hutchings, E. J. Samuelsen, and J. Skalyo, Jr., BNL Report, 1970 (unpublished).
[46]A. J. Sievers III and M. Tinkham, Phys. Rev. 129, 1566 (1963).
[47]J. R. Singer, Phys. Rev. 104, 929 (1956).
[48]P. W. Anderson, in *Magnetism*, edited by T. Rado and H. Suhl (Academic, New York, 1963), Vol. I, p. 25.
[49]P. W. Anderson, Phys. Rev. 115, 2 (1959).
[50]T. N. Casselman and F. Keffer, Phys. Rev. Letters 4, 498 (1960).
[51]L. C. Bartel, Phys. Rev. B 1, 1254 (1970).
[52]B. Morosin, Phys. Rev. B 1, 236 (1970).
[53]H. W. White, J. W. Battles, and G. E. Everett, Solid State Commun. 8, 313 (1970).
[54]J. G. Adler and T. T. Chen, Solid State Commun. 9, 501 (1971).
[55]D. C. Tsui, R. E. Dietz, and L. R. Walker, Phys. Rev. Letters 27, 1729 (1971).
[56]See M. T. Hutchings and H. J. Guggenheim, J. Phys. C 3, 1303 (1970), and references therein.
[57]H. A. Alperin, J. Phys. Soc. Japan Suppl. 17, 12 (1962); Phys. Rev. Letters 6, 55 (1961).
[58]B. E. F. Fender, A. J. Jacobson, and F. A. Wedgwood, J. Chem. Phys. 48, 990 (1968).
[59]E. J. Samuelsen and G. Shirane, Phys. Status Solidi 42, 241 (1970).
[60]J. S. Smart, *Effective Field Theories in Magnetism* (Saunders, Philadelphia, 1966).
[61]W. Low and R. S. Rubins, in *Paramagnetic Resonance*, edited by W. Low (Academic, New York, 1963), Vol. 1, p. 84.

PHYSICAL REVIEW B VOLUME 6, NUMBER 9 1 NOVEMBER 1972

Phase Transitions and Static Spin Correlations in Ising Models with Free Surfaces

K. Binder*
Physik-Department E 14, TUM, 8046 Garching bei München, BD Germany

and

P. C. Hohenberg
Theoretische Physik, TUM, 8046 Garching bei München, BD Germany, and Bell Laboratories, † Murray Hill, New Jersey 07974

(Received 17 April 1972)

Phase transitions in Ising models with free surfaces are studied from various points of view, including a phenomenological Landau theory, high-temperature series expansions, and a scaling theory for thermodynamic quantities and correlation functions. In the presence of a surface a number of new critical exponents must be defined. These arise because of the existence of "surface" terms in the thermodynamic functions, and because of the anisotropy of space and lack of translational symmetry introduced by the surface. The need for these new critical exponents already appears in the phenomenological theory, which is discussed in detail and related to the microscopic mean-field approximation. The essential new parameter appearing in this theory is an extrapolation length λ which enters the boundary condition on the magnetization at the surface. For magnetic systems this length is of the order of the interaction range, in contrast to superconductors, where it is usually much larger. In order to go beyond the mean-field theory, high-temperature series expansions are carried out for the Ising half-space, to tenth order in two dimensions and to eighth order in three dimensions. A scaling theory is developed both for thermodynamic functions and for spin correlations near the surface, and relations are found among the exponents of the half-space. Both the scaling theory and the numerical calculations are compared with the exact solution of the Ising half-plane (two dimensions) by McCoy and Wu, and agreement is found wherever the theory is applicable. In analogy to the bulk situation, the scaling theory is found to agree with mean-field theory in four dimensions. The prediction of the present work which is most easily accessible to experiment is the temperature dependence of the magnetization at the surface, with critical exponent estimated to be $\beta_1 = 2/3$. The mean-field result, $\beta_1 = 1$, seems to agree more closely with presently available experiment, and more work is needed to clarify the situation.

I. INTRODUCTION

Phase transitions in magnetic systems have been studied extensively both theoretically and experimentally in recent years.[1-3] Although experiments are carried out on finite systems with real surfaces, the theoretical models used for calculations have nearly always been infinite in extent. The usual justification for neglecting surface effects is that these only involve a fraction of order $N^{(d-1)/d}$ of the total number of atoms N, and this fraction is vanishingly small for large N (d is the